Applied Thermal Engineering 231 (2023) 120849

Contents lists available at ScienceDirect

Applied Thermal Engineering

journal homepage: www.elsevier.com/locate/apthermeng

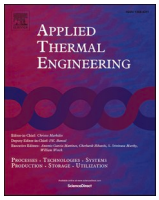

Research Paper

Performance analysis of sCO_2 tube with high non-uniform heat flux: Thermal-fluid-structural evaluation and optimization

Shuo Gao [a], Yanjuan Wang [a,*], Yi Li [a], Qibin Liu [b,c], Jinliang Xu [a]

[a] The Beijing Key Laboratory of Multiphase Flow and Heat Transfer, North China Electric Power University, Beijing 102206, China
[b] Institute of Engineering Thermophysics, Chinese Academy of Sciences, Beijing 100190, China
[c] University of Chinese Academy of Sciences, Beijing 10049, China

ARTICLE INFO

Keywords:
Supercritical CO_2 power systems
High non-uniform heat flux
Multi-physical coupling
Tube optimization

ABSTRACT

A supercritical carbon dioxide (sCO_2) tube is an important component in a sCO_2 power system for a wide range of heat sources. The sCO_2 tubes experience high temperature and pressure with high non-uniform heat flux when fossil fuel and solar energy are used as heat sources. Herein, a novel tube structure is proposed to match the circumferential thermal resistance with the non-uniform heat flux by changing the Eccentricity. A three-dimensional multi-physical coupling model was constructed to compare the proposed structure with a conventional tube. The fluid dynamics, thermal stress, and coupled heat transfer characteristics were analyzed, and the key working parameters were explored. The maximum temperature of the proposed structure was effectively reduced by 13–36 K and the maximum thermal stress was significantly reduced by approximately 25–33% under all the simulated working conditions when the Eccentricity changed from 0 to 0.4. The proposed novel structure will facilitate the safety and conserve tube material, and the results can serve as a reference for the development of sCO_2 power systems for industrial applications.

1. Introduction

Considering the importance of carbon neutrality, it is essential to develop efficient power conversion systems. Owing to its higher efficiency, compact system layout, and inertness, the sCO_2 Brayton cycle is a promising power cycle and alternative to the conventional steam Rankine cycle in fossil fuel power plants and has considerable potential for solar and nuclear energy applications [1–3]. The expected power generation efficiency of a sCO_2 coal-fired power plant can be improved by 6–7%, while the sCO_2 tube in the sCO_2 boiler is under high non-uniform heat flux (NUH) along the width, depth, and height of the furnace [4]. As solar power towers achieve higher temperatures, greater solar-to-electric efficiencies are obtained compared to those obtained by parabolic trough collectors. A solar power tower is a promising technology in the mid-term [5]. A sCO_2 solar power tower system can effectively improve efficiency, while the solar receivers must be subjected to non-uniform heat flux with a peak heat flux of up to 1.0 MW/m^2, which leads to a large temperature gradient and may cause tube deformation [6]. Thus, it is necessary to improve the receiver durability of non-uniform heating.

The sCO_2 tube is an important component in sCO_2 power systems for a wide range of heat sources, where it is subjected to high temperatures and pressures with a high NUH, which is far from the pseudo-critical point. The characteristics of sCO_2 flow and heat transfer in the subcritical state and near the pseudo-critical region have been widely investigated, especially for enhanced or deteriorated heat transfer near the pseudo-critical region. In contrast, the investigation of sCO_2 flow and heat transfer under high temperatures and pressures far from the pseudo-critical point is limited, which is important for the design of the receiver in solar power plants and the sCO_2 boiler in fossil fuel power plants.

For a coal-fired power plant, the heat load of the sCO_2 boiler is several times that of a traditional steam boiler [4]. However, the convective heat transfer coefficient of sCO_2 is lower [7], and the working temperature is higher [8]. Therefore, ensuring safety of the sCO_2 boiler is a challenging problem [9]. Cooling walls are key components of sCO_2 boilers, and their thermal–hydraulic performance is of increasing interest. Wang [10] developed a two-dimensional mathematical model that neglected the circumferential NUH. It was determined that the maximum temperature of the sCO_2 cooling wall tubes was much higher than that of the water wall tube, leading to larger tube deformation. Hence, a low inclination angle, an increase in the tube number, and a larger tube diameter were recommended to reduce the

* Corresponding author.
E-mail address: 90102184@ncepu.edu.cn (Y. Wang).

https://doi.org/10.1016/j.applthermaleng.2023.120849
Received 27 February 2023; Received in revised form 28 April 2023; Accepted 21 May 2023
Available online 24 May 2023

Nomenclature

C_p	specific heat capacity, J·kg^{-1}· K^{-1}
e	eccentric distance, mm
E_c	Eccentricity
E	elastic modulus, MPa
G	mass flux, kg·s^{-1}·m^{-2}
i	enthalpy, kJ·kg^{-1}
L	tube length, m
NUH	non-uniform heat flux
P	working pressure, MPa
q	heat flux, kW·m^{-2}
r	tube inner radius, mm
R	tube outer radius, mm
T	temperature, K
ΔT	temperature difference, K

Greek symbols

α	circumferential angle, ° or thermal expansion coefficient, K^{-1}
σ_{as}	allowable stress, MPa
λ	thermal conductivity, W·m^{-1}·K^{-1}
υ	poisson's ratio
ρ	density, kg·m^{-3}
σ_{eq}	equivalent stress, MPa
σ_p	mechanical stress, MPa
$\sigma_{t,max}$	maximum thermal stress, MPa
φ	view factor

Subscripts

ave	average
in	inlet
max	maximum
r, θ, l	radial, tangential, longitudinal direction
ref	reference
t	thermal
w	tube wall

temperature and pressure drop. To reduce the maximum temperature and the circumferential temperature difference of the cooling wall tube. Zhou et al. [11] proposed a novel furnace structure to lower the heat duty of the sCO_2 boiler. Liu et al. [12] introduced flue gas recirculation to reduce the heat flux density. These measures effectively lowered the boiler heat flux. To further improve the thermal–hydraulic performance, a symmetric flow pattern [11], cold sCO_2-hot fire matching, a cascaded temperature control principle [13], and improvement of the coupling between the non-uniform heat flux and cooling wall tubes along the width and height directions [12] were proposed to optimize the coupling between the heat flux in the furnace and the cooling wall tubes. To further improve the comprehensive performance, several heat transfer structures and processes for fabricating them were proposed. These included the use of internal spiral finned tubes [14] and the insertion of internal twisted tapes in the tube [15], which can effectively boost the thermal performance while with serious resistance increase.

Herein, a novel structure is proposed that considers comprehensive factors such as heat transfer, flow resistance, and thermal stress. The new structure matches the circumferential non-uniform heat flux with the circumferential thermal resistance of the tube. A thermal-fluid-mechanical coupling model with high NUH is developed to analyze the performance of the proposed structure and a traditional structure in Section 2. In Section 3, the characteristics of the proposed and traditional structures is compared. The performance of the proposed structure with respect to heat flux(q), mass flux (G), working pressure (P), and tube length (L) is then numerically investigated. Finally, the main conclusions are presented in Section 4.

2. Numerical model and method

2.1. Physical model

Considering the complexity of the cooling wall and the similarity of the heat flux distribution on the surface of each tube, a single tube of 1 m was chosen as the physical model to facilitate modeling and simplification of the calculations. It was a seamless steel tube made of 316H material with outer (R) and inner radius (r) of 17.5 mm and 11 mm respectively, (Fig. 1). Gravity is contrary to the sCO_2 flow direction. A circumferential NUH was applied on the outer tube wall and the circumferential angle (α) at the bottom was 180°.

A novel structural tube is proposed (Fig. 2). For the novel structural, the upper half circular of the outer wall of the traditional tube (as shown in blue Fig. 2(b)) is moved downwards by a distance of e (eccentric distance) while keeping the lower half circle unchanged, and their intersection is obtained. Thus, the tube wall thickness of the heat-absorbing side was reduced, whereas the wall thickness of the back-side did not change. These modifications allowed the low thermal conduction resistance to match the high heat flux.

2.2. Governing equations and boundary conditions

2.2.1. Thermal-fluid calculation of sCO_2

A three-dimensional model was developed to study the flow and heat transfer process. Owing to the low relative errors in our previous study [10], the k-ε model was adopted. The characteristics of the cooling wall are governed by the continuity equation, energy equation, and momentum equation, which are as follows:

Continuity equation:

$$\frac{\partial}{\partial x_i}(\rho u_i) = 0 \tag{1}$$

Energy equation:

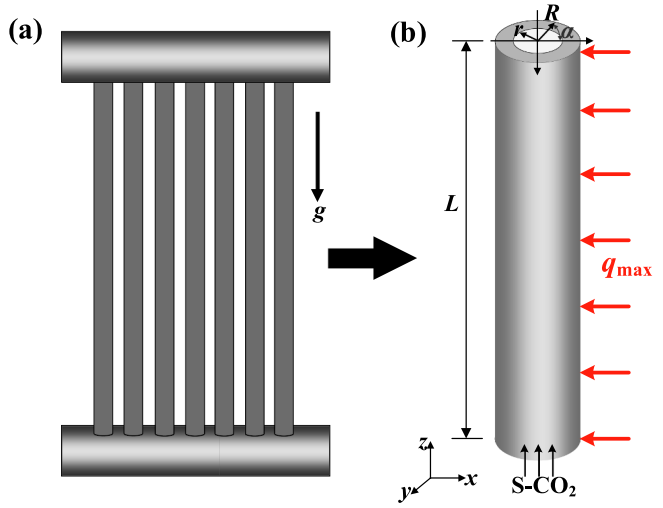

(a) Arrangement in boiler (b) Physical configuration

Fig. 1. Schematic of cooling wall tube in sCO_2 boiler. (a) Arrangement in boiler (b) Physical configuration.

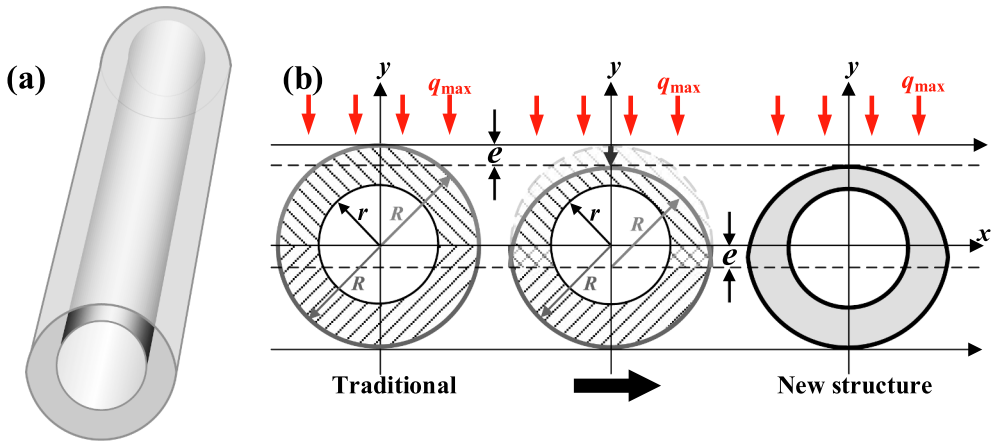

(a) Three-dimensional structure (b) Construction process of the proposed tube

Fig. 2. The proposed tube structure. (a) Three-dimensional structure (b) Construction process of the proposed tube.

$$\rho C_p u_i \frac{\partial T}{\partial x_i} = (\lambda + \lambda_T)\frac{\partial}{\partial x_i}\left(\frac{\partial T}{\partial x_i}\right) \tag{2}$$

Momentum equation:

$$\frac{\partial}{\partial x_j}(\rho u_i u_j) = -\frac{\partial p}{\partial x_i} + \frac{\partial}{\partial x_j}\left[(\mu + \mu_t)\left(\frac{\partial u_i}{\partial x_j} + \frac{\partial u_j}{\partial x_i}\right) - \frac{2}{3}(\mu + \mu_t)\frac{\partial u_i}{\partial x_i}\delta_{ij} - \frac{2}{3}\rho k\delta_{ij}\right] + F \tag{3}$$

The k-ε model introduces two additional transport equations and two dependent variables: the turbulent kinetic energy, k, and the turbulent dissipation rate, ε. The transport equation for k is as follows:

$$\frac{\partial \rho k}{\partial t} + U_j\frac{\partial \rho k}{\partial x_j} = \tau_{ij}\frac{\partial U_i}{\partial x_j} - \rho\varepsilon + \frac{\partial}{\partial x_j}\left[\left(\mu + \frac{\mu_t}{\sigma_k}\right)\frac{\partial k}{\partial x_j}\right] \tag{4}$$

The transport equation for ε is as follows:

$$\frac{\partial \rho\varepsilon}{\partial t} + U_j\frac{\partial \rho\varepsilon}{\partial x_j} = C_{\varepsilon 1}\frac{\varepsilon}{k}\tau_{ij}\frac{\partial U_i}{\partial x_j} - C_{\varepsilon 2}\rho\frac{\varepsilon^2}{k} + \frac{\partial}{\partial x_j}\left[\left(\mu + \frac{\mu_i}{\sigma_\varepsilon}\right)\frac{\partial \varepsilon}{\partial x_j}\right] \tag{5}$$

The turbulent viscosity is modeled as follows:

$$\mu_t = \frac{\rho C_\mu k^2}{\varepsilon} \tag{6}$$

where $C_\mu = 0.09$, $C_{\varepsilon 1} = 1.44$, $C_{\varepsilon 2} = 1.92$, $\sigma_k = 1.0$ and $\sigma_\varepsilon = 1.3$. λ defines the thermal conductivity of the fluid; λ_T is the turbulent conductivity and C_p is the specific heat capacity.

The thermal-fluid boundary conditions are specified as follows: Inlet: $u = u_{in}$ (a fully developed flow velocity, which has a parabolic velocity profile), T = 773.15 K, and P = 25 MPa; Outlet: fully-developed assumption [16]; The solid–fluid interfaces: the wall function boundary condition is used [17], and a theoretical lift-off δ_w from the physical wall is assumed. Expressed in viscous units, the wall lift-off is defined as follows:

$$\delta_w^+ = \max\left(\frac{h_w}{2}\frac{\rho C_\mu^{1/4}\sqrt{k}}{\mu}, 11.06\right) \tag{7}$$

The second argument is the distance from the wall, in viscous units. This lower limit ensures that the wall functions remain non-singular for all Reynolds numbers. The wall lift-off, δ_w, is defined as follows:

$$\delta_w = \frac{\delta_w^+ \mu}{\rho u_\tau} \tag{8}$$

where, h_w is the height of the mesh cell adjacent to the wall, and u_τ is the friction velocity [17].

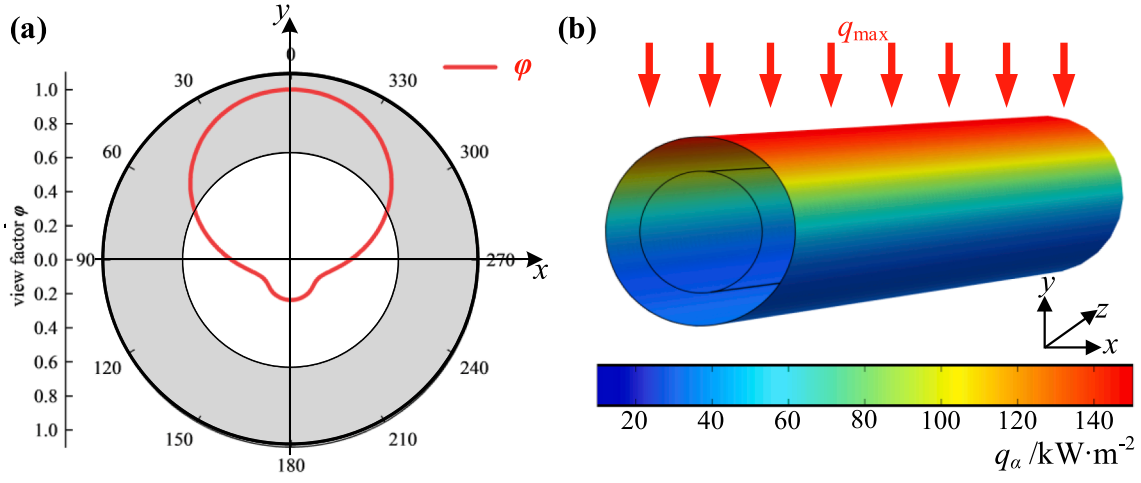

(a) Cross-section irradiation profile (b) NUH distribution.

Fig. 3. NUH distribution. (a) Cross-section irradiation profile (b) NUH distribution.

Table 1
Physical properties of 316H.

ρ, kg/m^3	7090
α, /K^{-1}	$1.43\times10^{-5}+7.34\times10^{-9}T-2.65\times10^{-12}T^2$
λ, W/(m·K)	21.5
E, Pa	$2.11\times10^{11}-3.59\times10^{7}T-3.75\times10^{4}T^2$
C_p, J/(kg·K)	500
υ	0.3

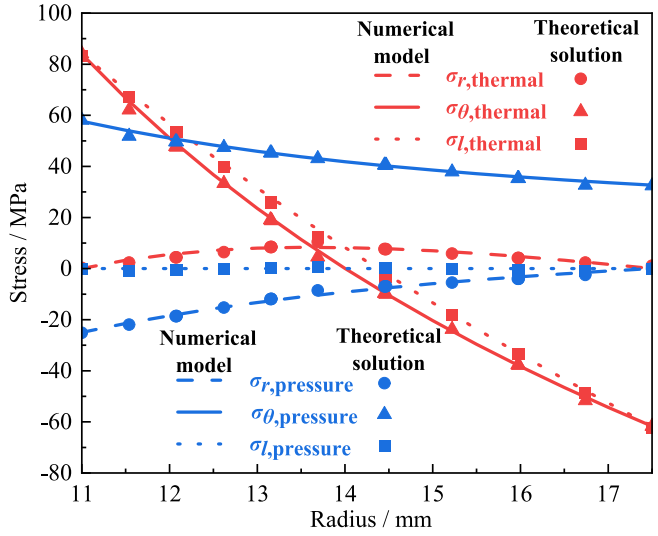

Fig. 4. Validation of structural model against theoretical solutions.

Only radiative heat transfer is considered in this model because the cooling wall tubes in the furnace are primarily heated by radiation from the flame [18]. The view factor (φ) is used to describe the circumferential non-uniform radiant heat flux distribution of the tube [19,20]. It is defined as the ratio of q_α to q_{max}, where q_{max} is the external effective radiant maximum heat flux and q_α is the heat flux at a specific angle around the outer wall of the cooling wall tube. The cross-section irradiation profile is shown in Fig. 3. Subsequently, the non-uniform radiative heat flux boundary conditions were used at the cooling wall tube's outer surface. The CO_2 properties as a function of temperature and pressure are provided by REFPROP [21].

2.2.2. Simulations of the cooling wall tube

Based on the operating conditions and data of the sCO_2 boiler, 316H was used as the tube material. The heat transfer of the cooling tube wall was via heat conduction and Table 1 lists its physical properties.

The structural analysis of the cooling tube is another significant concern for improving the safety and dependability of sCO_2 in coal-fired power plants. The governing equations of the thermal (σ_t), mechanical (σ_p), and equivalent stresses (σ_{eq}) are presented in [22,23]. The thermal and pressure loads are considered in the structural and stress analyses of the tube. First, the governing equations of the thermal-fluid are solved, and the pressure and temperature distributions are obtained. In practical applications, the pressure inside the sCO_2 boiler is low and is assumed to be 0 kPa [24]. Second, the static-structure equations are solved. The pressure and temperature distributions are imported as loading conditions, and the stress-free reference temperature is 293.15 K. The inlet end of the tube can expand along the flow direction only, and the outlet end is fixed with internal and external surfaces that are expandable. Subsequently, the thermal stress distribution and deformation of the tubes are obtained. The maximum residuals for all the governing equations were below 10^{-3} to ensure convergence of the calculations. To improve the accuracy of the simulation results, grid-independent check was conducted and the relative error was <0.01.

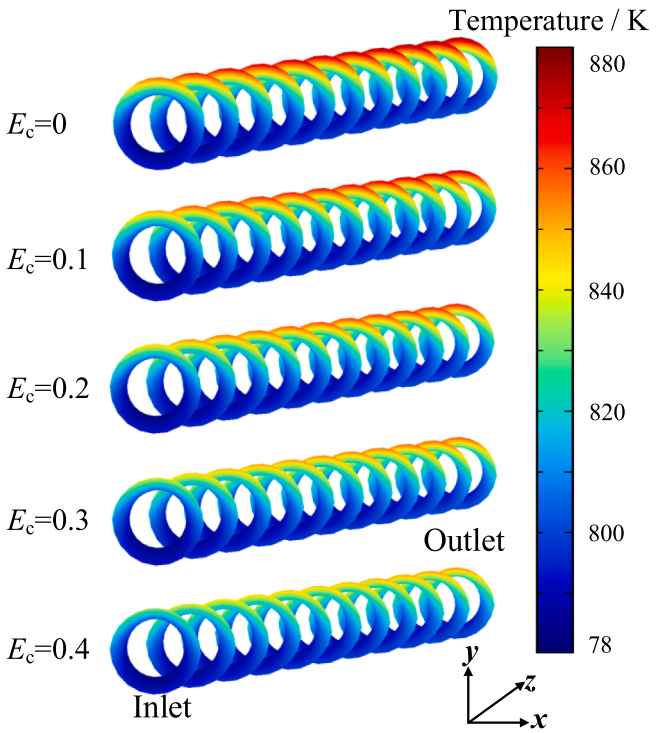

Fig. 5. Variations in cooling wall temperature with E_c.

2.3. Model validations

Owing to the lack of experimental data for the thermal-fluid-structural model calculations, the thermal-fluid model and the structural model were validated separately. The thermal-fluid model was verified by the experimental data provided by Zhu et al. [7] in our previous study [10]. The numerical mechanical model is verified with theoretical solutions [22]. The mechanical and thermal stress caused by the pressure load (25 MPa) and thermal load (temperature difference of 35.1 K) between the inner and outer wall were calculated by numerical and theoretical methods, respectively.

The calculation was performed in three principal directions: radial (r), tangential (θ), and longitudinal (l). The distribution of the mechanical and thermal stress along the radial direction are shown in Fig. 4. It is observed that the numerical results for different stresses are consistent with the theoretical solutions, which is indicative of the feasibility and accuracy of the structural model.

3. Results and discussions

3.1. Performance of the novel structure tube

The Eccentricity ($E_c = e/(R\text{-}r)$) was used to measure the non-uniformity of the thickness of the tube wall. The wall thickness of the fireside decreased with the increase of E_c. Thinner tube wall is good for the heat transfer process, however, it may cause safety concerns. Hence, the minimum safe thickness of the tubes under different working conditions was examined based on [25].

The characteristics of the proposed tubes with different Eccentricities are shown in Figs. 5 and 6. The conditions were defined as follows: the sCO_2 inlet mass flux, q_{max}, and sCO_2 inlet temperature (T_{in}) were 2000 kg/(m^{2}s), 150 kW/m^2, and 773.15 K, respectively.

Figs. 5 and 6 and Table 2 show that the temperature, thermal stress and volume of the proposed tubes decrease with the increase of E_c. In Fig. 5, it can be observed that the maximum cross section temperature appears at the heat-absorbing side (in the vicinity of $\alpha = 0°$), and is gradually increased along the flow direction. The maximum

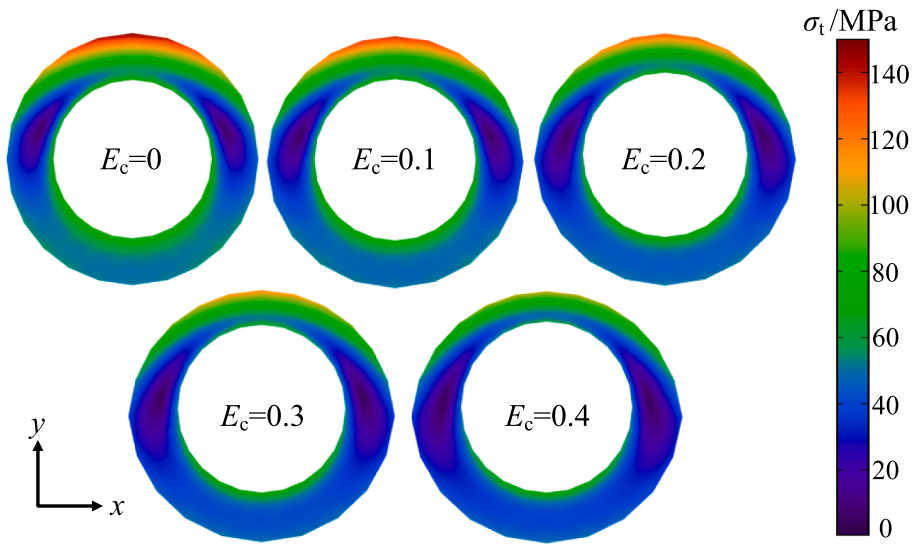

Fig. 6. Thermal stress profiles of the proposed tube at z = 0.5 m.

Table 2
Variations in tube volume with Eccentricity.

E_c	0	0.1	0.2	0.3	0.4
Volume/10^{-4} m^3	5.79	5.56	5.33	5.11	4.88
Reduced ratio/%	0.0	3.9	7.8	11.8	15.6

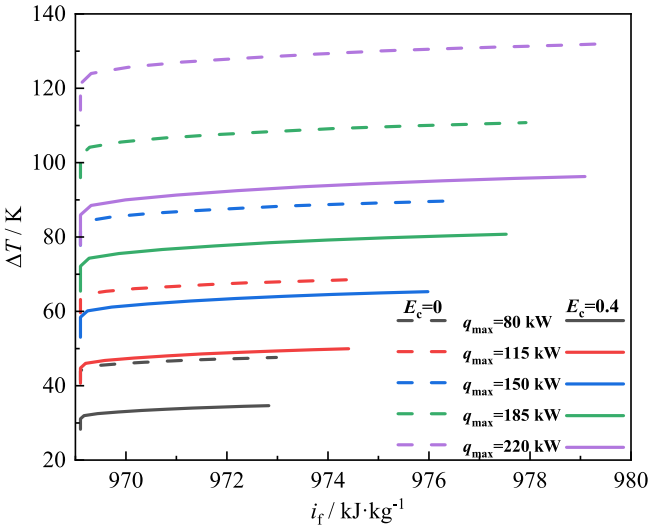

Fig. 7. ΔT as a function of E_c and q_{max}.

temperature (T_{max}) decreased from 879 K to 854.2 K, the maximum thermal stress ($\sigma_{t,max}$) decreased from 148 MPa to 105 MPa, and the material usage of the tube was conserved by approximately 15.6%, when the E_c increases from 0 (a traditional tube) to 0.4.

3.2. Effects of the key working parameters

The thermal performance of the proposed tube in relation to several working parameters, that affect the temperature and stress distribution, including heat flux, mass flux, working pressure, and tube length, is discussed in this section.

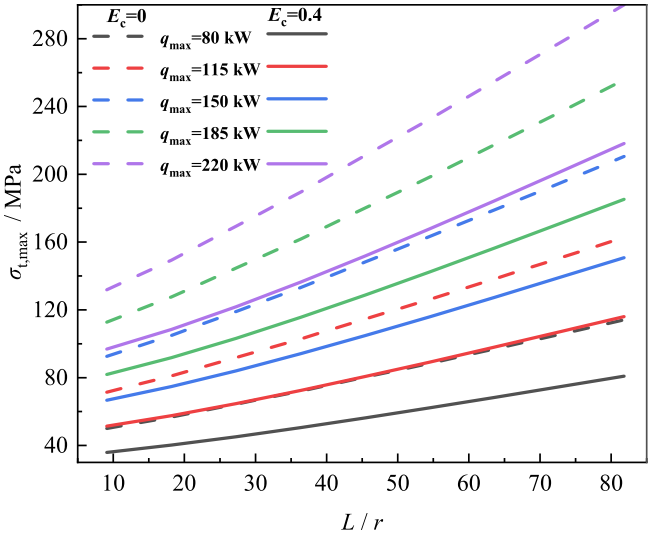

Fig. 8. $\sigma_{t,max}$ as a function of E_c and q_{max}.

3.2.1. Effects of heat flux

Figs. 7–10 illustrate the effects of E_c and heat flux on the performance of the cooling wall tube under typical working conditions, e.g., the sCO_2 inlet mass flux of 2000 kg/(m^{2}s), working pressure of 25 MPa, and sCO_2 inlet temperature of 773.15 K.

Fig. 7 shows ΔT (difference between the maximum and minimum temperature of cross-section) ~ i (enthalpy) curves with q_{max} and E_c. The outlet enthalpy increases with q_{max} as more heat is absorbed. ΔT increases along the flow direction, and the increasing trend gradually slows down. ΔT increases with q_{max} for both the traditional and novel structure tubes. When q_{max} is in the range of 80–220 kW/m^2, the maximum ΔT incresaes from 47.6 K to 132 K for a traditional tube. This indicates that q_{max} significantly influences ΔT. When E_c is 0.4, ΔT decreases significantly by 13–35.7 K (approximately 28.3%) compared with a traditional tube under all the simulated working conditions. In addition, the proposed tube exhibits excellent optimization, which increases with q_{max} in the case of the reduction of ΔT. The reduction in ΔT indicates a decrease in the thermal stress.

The variation of the maximum cross-sectional thermal stress is similar to that of ΔT, as shown in Fig. 8. $\sigma_{t,max}$ increases along the flow

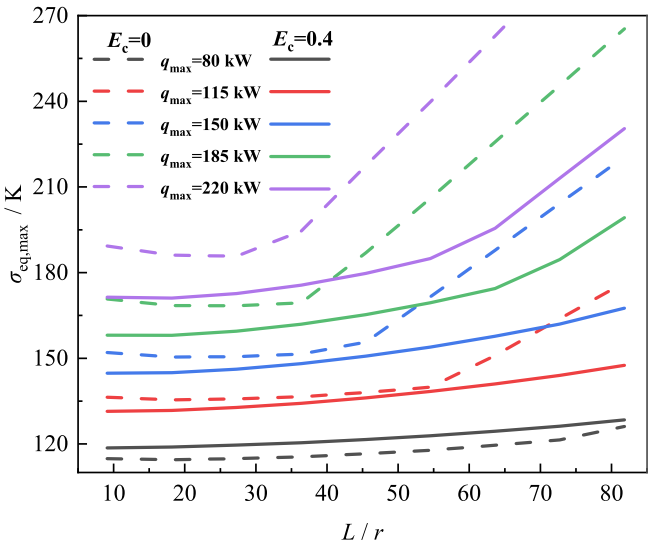

Fig. 9. $\sigma_{eq,max}$ as a function of E_c and q_{max}.

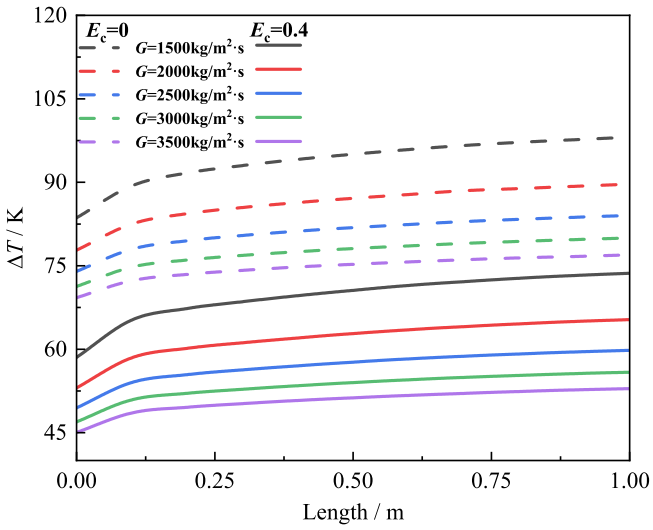

Fig. 11. ΔT as a function of E_c and G.

direction and also increases with q_{max} for both the traditional and novel structure tubes. When q_{max} is in the range of 80–220 kW/m^2, $\sigma_{t,max}$ increases from 114.1 MPa to 300 MPa for a traditional tube. When E_c is 0.4, $\sigma_{t,max}$ decreases significantly by 33.3–81.9 MPa (approximately 27.3–29.2%) compared to a traditional tube under all the simulated working conditions.

Fig. 9 shows that the variation of the maximum cross-sectional equivalent stress ($\sigma_{eq,max}$) is similar to $\sigma_{t,max}$ under high q_{max}. Whereas q_{max} is as low as 80 kW/m^2, $\sigma_{eq,max}$ of the novel structure is greater than that of the traditional tube because when q_{max} is low, the thermal stress decreases. Thus, mechanical stress dominates which increases with E_c, indicating that the novel structure is very effective in optimizing stress for high q_{max} working conditions.

Fig. 10 shows the influence of the heat flux and E_c on the maximum temperature of cooling wall tube. T_{max} increases with q_{max} for both the traditional and proposed tube as more heat is absorbed. In contrast, T_{max} decreases with the increase of E_c. In addition, T_{max} is significantly reduced by the proposed tube structure for all heat flux conditions. T_{max} decreases by 13–36 K when E_c increases from 0 to 0.4 under all the simulated working conditions. Therefore, a larger E_c does not only result in superior optimization in terms of $\sigma_{t,max}$, but also reduces T_{max} of the tube. This increases the maximum allowable stress (σ_{as}) and decreases δ_m, thereby further expanding the range of E_c in industrial design.

3.2.2. Effects of the mass flux

Fig. 11 illustrates the relationship between ΔT of the tube and the mass flux of the sCO_2 under typical working conditions, e.g., the sCO_2 inlet temperature of 773.15 K, q_{max} of 150 kW/m^2, and sCO_2 working pressure of 25 MPa.

Furthermore, ΔT decreases with increasing mass flux, whereas the decreasing trend gradually slows down. When the mass flux ranges from 1500 to 2000 kg/(m^{2}s), the maximum ΔT is reduced by approximately 8.6%. However, the maximum ΔT is only reduced by approximately 3.8% when the mass flux ranges from 2500 to 3000 kg/(m^{2}s) for the traditional tube. When E_c is 0.4, ΔT decreases significantly by approximately 24 K (~26–32%) compared to the traditional tube under all simulated conditions. The proposed tube shows excellent optimization in terms of the reduction of ΔT, which increases with the mass flux.

Fig. 12 shows the influence of E_c and G on T_{max}. T_{max} decreases with an increase in the mass flux, and the decreasing trend gradually slows down. T_{max} is reduced by the proposed tube structure and decreases by 24 K (~2.8%) for the different mass fluxes when E_c increases from 0 to 0.4. The results indicate that the optimization effect of the proposed tube is applicable to different mass flux conditions and is not affected by the mass flux.

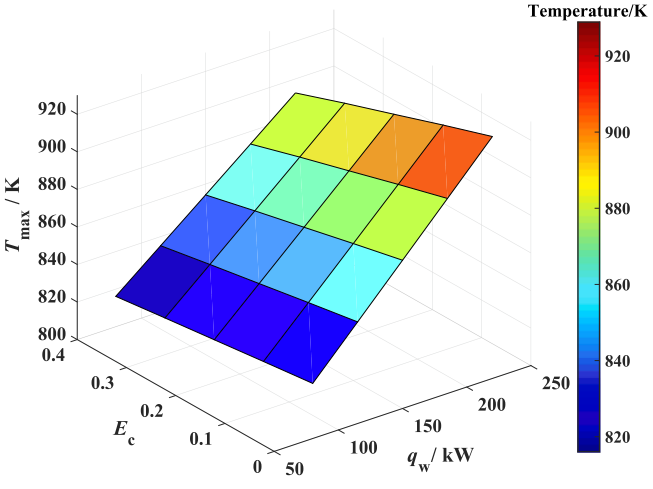

Fig. 10. T_{max} as a function of E_c and q_{max}.

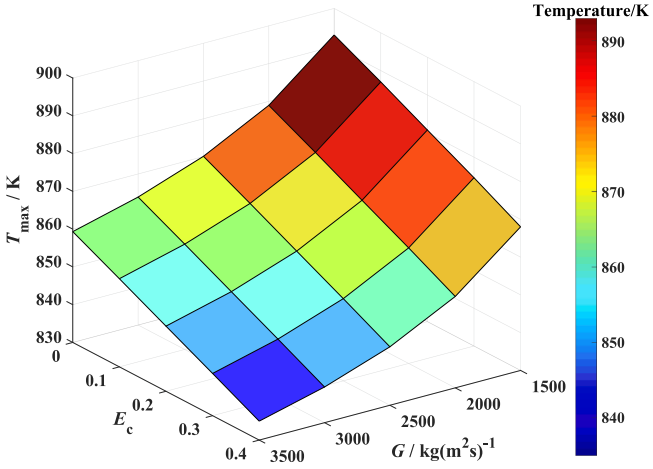

Fig. 12. T_{max} as a function of E_c and G.

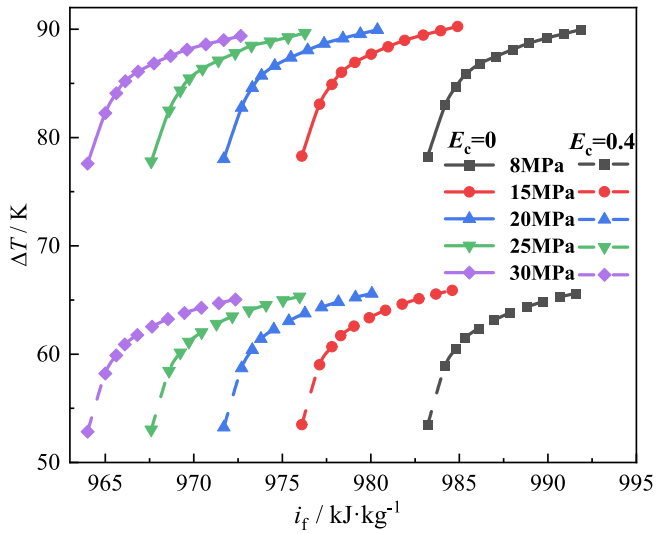

Fig. 13. Variations of ΔT with E_c and P.

3.2.3. Effects of working pressure

Fig. 13 shows ΔT~i curves with P and E_c when the sCO_2 inlet mass flux, q_{max}, and inlet temperature are 2000 kg/(m^{2}s), 150 kW/m^2, and 773 K, respectively. ΔT increases along the flow direction, and the increasing trend gradually slows down. The temperature change is similar for the different pressures. This may be because λ of sCO_2 is only slightly affected by P. The maximum ΔT can reach 90 K when E_c is 0. Moreover, ΔT is significantly reduced by the proposed tube structure at all pressures and decreases by 24.3 K (~28%) when E_c increases from 0 to 0.4.

Fig. 14 shows the influence of P and E_c on the T_{max} of the cooling wall tube. P has a small effect on T_{max}, which is significantly reduced by the proposed tube structure at all pressures. T_{max} is reduced by approximately 24.8 K when E_c increases from 0 to 0.4. This indicates that the optimization effect of the proposed tube on T_{max} is applicable to different pressure conditions and the optimization effect is not affected by the working pressure. When the working pressure is low, δ_m can be decreased further. Thus, σ_t and T_{max} can be reduced further.

3.2.4. Effects of the tube length

Figs. 15 and 16 illustrate the effects of E_c and L on the cooling wall tube performance under typical working conditions, e.g., the sCO_2 inlet mass flux of 2000 kg/(m^{2}s), working pressure of 25 MPa, and sCO_2 inlet temperature of 773.15 K.

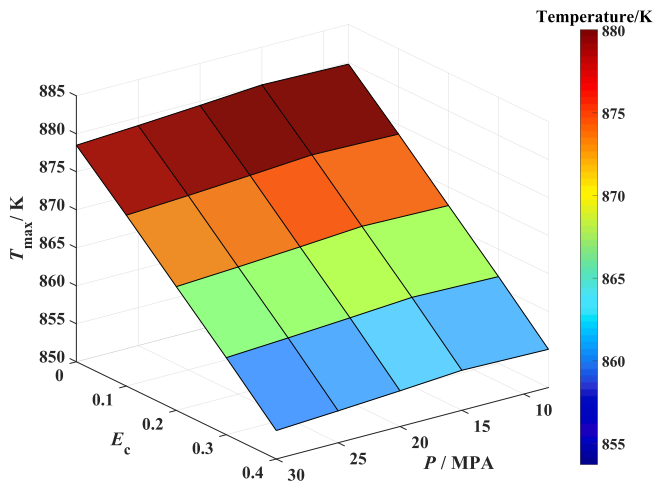

Fig. 14. Variations of T_{max} with E_c and P.

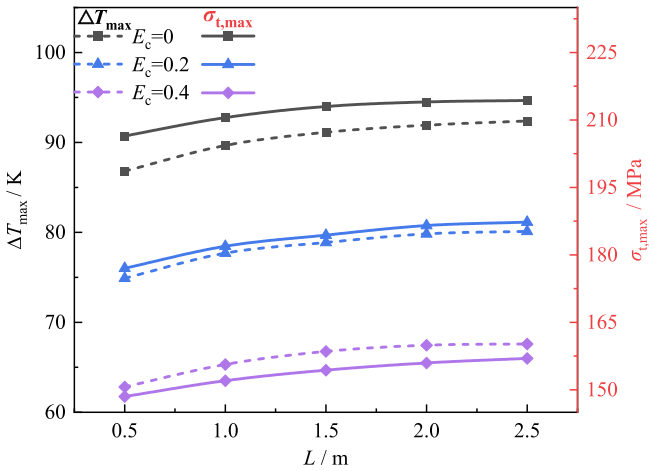

Fig. 15. Variations in ΔT_{max} and $\sigma_{t,max}$ with E_c and L.

Fig. 15 shows the variation of the maximum cross-sectional temperature difference (ΔT_{max}) for different E_c and tube lengths. ΔT_{max} increases with L, however, the increasing trend gradually slows down. This may be attributed to the poor heat transfer between sCO_2 and the tube wall because the sCO_2 temperature increases with L. When L is in the range of 0.5–2.5 m, ΔT_{max} is increased by 5.6 K (7%). Moreover, ΔT_{max} is significantly reduced by the proposed tube structure for all tube length conditions and is reduced by approximately 24 K (~27%) when E_c increases from 0 to 0.4. Fig. 15 shows that variations of $\sigma_{t,max}$ are similar to those of ΔT_{max}. $\sigma_{t,max}$ is reduced by approximately 58 MPa (~27%) when E_c increases from 0 to 0.4.

Fig. 16 shows the effect of E_c and L on T_{max}. It is observed that T_{max} increases with the tube length. T_{max} increases by approximately 20 K when L changes from 0.5 m to 2.5 m and is reduced when E_c increases. The reduction in T_{max} is similar for different tube lengths. T_{max} decreases by approximately 25 K when E_c increases from 0 to 0.4. This implies that the optimization effect of the proposed tube on T_{max} is applicable to various tube length conditions, and the optimization is not affected by the tube length. The reduction of T_{max} plays a crucial role in extending the service life of the cooling wall tube and improving operational safety.

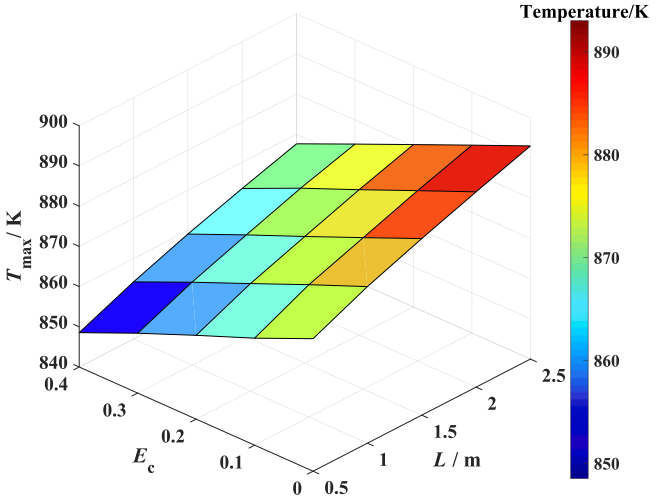

Fig. 16. T_{max} as a function of E_c and L.

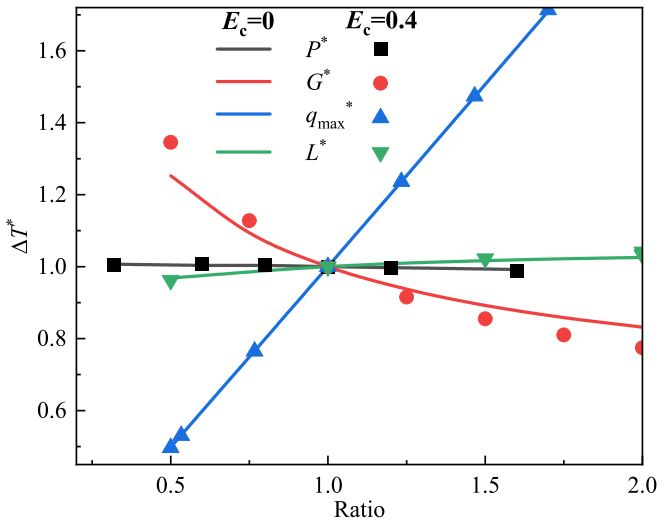

Fig. 17. Changes in ΔT^* with P^*, G^*, L^*, and $q_{max}{}^*$ at $E_c = 0$ and 0.4.

4. Sensitivity analysis

Sensitivity analysis of the parameters is critical in the design of the cooling wall. The following approach uses the one-at-a-time method, which is one of the most common sensitivity methods [26]. In the reference case, the parameters were P_{ref} = 25 MPa, G_{ref} = 2000 kg/(m^2s), L_{ref} = 1 m, and $q_{max,ref}$ = 150 kW/m^2. The maximum temperature difference calculated under this working condition is used as the reference value ($\Delta T_{max,ref}$). Each parameter was varied one-at-a-time, then calculate the maximum temperature difference ΔT_{max} under this working condition and divide it by the $\Delta T_{max,ref}$ to obtain the ratio ΔT^*. When a parameter changes, its ratio to the corresponding parameter in the reference case is "*", while other parameters remain unchanged. For example, when exploring the sensitivity of P, the magnitude of P changes and the ratio is $P^* = P/P_{ref}$. The calculation results for different working conditions are illustrated in Fig. 17.

The variation of the proposed and traditional tubes is similar. When P^* increases from 0.32 to 1.6 and ΔT^* decreases from 1.01 to 0.99. When L^* increases from 0.5 to 2, ΔT^* increases from 0.97 to 1.03. When $q_{max}{}^*$ increases from 0.5 to 1.7, ΔT^* increases from 0.5 to 1.71. While the influence of G on ΔT differs in the case of the proposed tube and the traditional tube, when G^* increases from 0.5 to 2, ΔT^* decreases from 1.25 to 0.83 for the traditional tube and 1.35 to 0.77 for the proposed tube. Thus, the effect of mass flux on ΔT increases with E_c. Additionally, both P and G negatively influence ΔT, whereas L and q_{max} positively influence ΔT with q_{max} more significantly than the others, and G has a greater effect than L, and P has the least effect.

5. Conclusions

The thermal-fluid-structural characteristics of a sCO_2 tube with high non-uniform heat flux were numerically investigated, and a novel structure tube was proposed to improve the comprehensive performance. The thermal performance of the proposed tube in relation to key working parameters was discussed. The main conclusions are as follows.

(1) The variation of the temperature, thermal stress, and tube volume with the Eccentricity was obtained. They all decrease with the increase of Eccentricity. The tube material can be conserved by approximately 15.6%, when the Eccentricity increases from 0 to 0.4.

(2) The maximum temperature and equivalent stress decreases with the mass flux and increase with the heat flux and tube length for both the traditional and the proposed tubes, whereas the working pressure has little effect on them. The novel structure is very effective in optimizing stress for high non-uniform heat flux working conditions.

(3) A sensitive analysis revealed that the major influencing factor is heat flux, followed by mass flux, tube length, and working pressure. When the Eccentricity is 0.4, the maximum temperature of the novel structure is reduced by 13–36 K; the maximum temperature difference is reduced by 26–32%, and the maximum thermal stress is reduced by approximately 25–33% compared to the traditional structure under all the simulated working conditions.

The results can serve as a fundamental reference for the design and optimization of the sCO_2 tube under high non-uniform heat flux and promote the development of sCO_2 power systems in industrial applications.

Declaration of Competing Interest

The authors declare that they have no known competing financial interests or personal relationships that could have appeared to influence the work reported in this paper.

Data availability

No data was used for the research described in the article.

Acknowledgements

The authors appreciate the financial support provided by the National Natural Science Foundation of China (52076075 and 52130608)

References

[1] G. Liao, L. Liu, J. E, F. Zhang, J. Chen, Y. Deng, H. Zhu, Effects of technical progress on performance and application of supercritical carbon dioxide power cycle: A review, Energy Convers, Manage 199 (2019) 111986.
[2] J.H. Park, H.S. Park, J.G. Kwon, T.H. Kim, M.H. Kim, Optimization and thermodynamic analysis of supercritical CO2 Brayton recompression cycle for various small modular reactors, Energy 160 (2018) 520–535.
[3] M. Mehrpooya, P. Bahramian, F. Pourfayaz, M.A. Rosen, Introducing and analysis of a hybrid molten carbonate fuel cell-supercritical carbon dioxide Brayton cycle system, Sustainable Energy Technol. Assess. 18 (2016) 100–106.
[4] J. Xu, E. Sun, M. Li, H. Liu, B. Zhu, Key issues and solution strategies for supercritical carbon dioxide coal fired power plant, Energy 157 (2018) 227–246.
[5] R.P. Merchán, M.J. Santos, A. Medina, A. Calvo Hernández, High temperature central tower plants for concentrated solar power: 2021 overview, Renew. Sustain. Energy Rev. 155 (2022) 111828.
[6] B. Du, Y. He, Z. Zheng, Z. Cheng, Analysis of thermal stress and fatigue fracture for the solar tower molten salt receiver, Appl. Therm. Eng. 99 (2016) 741–750.
[7] B. Zhu, J. Xu, X. Wu, J. Xie, M. Li, Supercritical "boiling" number, a new parameter to distinguish two regimes of carbon dioxide heat transfer in tubes, Int. J. Therm. Sci. 136 (2019) 254–266.
[8] H. Li, Y. Zhang, M. Yao, Y. Yang, W. Han, W. Bai, Design assessment of a 5 MW fossil-fired supercritical CO2 power cycle pilot loop, Energy 174 (2019) 792–804.
[9] K. Brun, P. Friedman, R. Dennis, Fundamentals and Applications of Supercritical Carbon Dioxide (sCO2) Based Power Cycles, Woodhead publishing, 2017.
[10] Y. Wang, B. Yu, S. Gao, Q. Liu, J. Xu, performance analysis of cooling wall of supercritical CO2 coal-fired plants, J. Therm. Sci. 31 (2022) 1881–1890.
[11] J. Zhou, M. Zhu, K. Xu, S. Su, Y. Tang, S. Hu, Y. Wang, J. Xu, L. He, J. Xiang, Key issues and innovative double-tangential circular boiler configurations for the 1000 MW coal-fired supercritical carbon dioxide power plant, Energy 199 (2020) 117474.
[12] C. Liu, J. Xu, M. Li, Q. Wang, G. Liu, The comprehensive solution to decrease cooling wall temperatures of sCO2 boiler for coal fired power plant, Energy 252 (2022) 124021.
[13] D. Yang, G. Tang, Y. Fan, X. Li, S. Wang, Arrangement and three-dimensional analysis of cooling wall in 1000 MW S–CO_2 coal-fired boiler, Energy 197 (2020) 117168.
[14] J. Muñoz, A. Abánades, Analysis of internal helically finned tubes for parabolic trough design by CFD tools, Appl. Energy 88 (2011) 4139–4149.
[15] X. Li, G. Tang, D. Yang, Y. Fan, J. Xu, Thermal-hydraulic-structural evaluation of S–CO_2 cooling wall tubes: A thermal stress evaluating criterion and optimization, Int. J. Therm. Sci. 170 (2021) 107161.
[16] S.V. Patankar, Numerical Heat Transfer and Fluid Flow, CRC Press, 2018.
[17] D.C. Wilcox, Turbulence Modeling for CFD, 2nd ed., DCW Industries, 1998.

[18] E. Sun, J. Xu, M. Li, G. Liu, B. Zhu, Connected-top-bottom-cycle to cascade utilize flue gas heat for supercritical carbon dioxide coal fired power plant, Energ. Conver. Manage. 172 (2018) 138–154.
[19] P. Duda, J. Taler, A new method for identification of thermal boundary conditions in water-wall tubes of boiler furnaces, Int. J. Heat Mass Transf. 52 (2009) 1517–1524.
[20] J. Taler, P. Duda, B. Węglowski, W. Zima, S. Grądziel, T. Sobota, D. Taler, Identification of local heat flux to membrane water-walls in steam boilers, Fuel 88 (2009) 305–311.
[21] E.W. Lemmon, M.L. Huber, M.O. McLinden, 2010. NIST Standard Reference Database 23, Reference Fluid Thermodynamic and Transport Properties (REFPROP), version 9.0, National Institute of Standards and Technology. File dated December, 22: 2010.
[22] T.W. Neises, M.J. Wagner, A.K. Gray, Asme, Structural Design Considerations for Tubular Power Tower Receivers Operating at 650°C, in: ASME 8th International Conference on Energy Sustainability, Seaport World Trade Ctr, Boston, MA, 2014.
[23] K. Wang, P. Jia, Y. Zhang, Z. Zhang, T. Wang, C. Min, Thermal-fluid-mechanical analysis of tubular solar receiver panels using supercritical CO2 as heat transfer fluid under non-uniform solar flux distribution, Sol. Energy 223 (2021) 72–86.
[24] J. Wang, X. Chen, C. Zhang, M. Gu, H. Chu, Numerical Investigation of Heat Transfer Characteristics of Supercritical CO_2 Tube in Combustion Chamber of Coal-Fired Boiler, J. Therm. Sci. 28 (2019) 442–453.
[25] J.D. Ortega, J.M. Christian, C.K. Ho, Asme, Structural Analysis of a Direct Heated Tubular Solar Receiver for Supercritical CO2 Brayton Cycle, in: 9th ASME International Conference on Energy Sustainability, San Diego, CA, 2015.
[26] J.M. Murphy, D.M. Sexton, D.N. Barnett, G.S. Jones, M.J. Webb, M. Collins, D. A. Stainforth, Quantification of modelling uncertainties in a large ensemble of climate change simulations, Nature 430 (2004) 768–772.